Published in final edited form as:
Cancer Lett. 2013 September 1; 337(2): 254–265. doi:10.1016/j.canlet.2013.04.034.

Synergistic Combination Therapy with Nanoliposomal C6-Ceramide and Vinblastine is Associated with Autophagy Dysfunction in Hepatocarcinoma and Colorectal Cancer Models

Pavan P. Adiseshaiah[1], **Jeffrey D. Clogston**[1], **Christopher B. McLeland**[1], **Jamie Rodriguez**[1], **Timothy M. Potter**[1], **Barry W. Neun**[1], **Sarah L. Skoczen**[1], **Sriram S. Shanmugavelandy**[2], **Mark Kester**[2], **Stephan T. Stern**[1], and **Scott E. McNeil**[1]

[1]Nanotechnology Characterization Laboratory, Advanced Technology Program, SAIC-Frederick, Inc., Frederick National Laboratory for Cancer Research, Frederick, MD 21702

[2]Department of Pharmacology, Pennsylvania State University College of Medicine, Hershey, PA 17033

Abstract

Autophagy, a catabolic survival pathway, is gaining attention as a potential target in cancer. In human liver and colon cancer cells, treatment with an autophagy inducer, nanoliposomal C6-ceramide, in combination with the autophagy maturation inhibitor, vinblastine, synergistically enhanced apoptotic cell death. Combination treatment resulted in a marked increase in autophagic vacuole accumulation and decreased autophagy maturation, without diminution of the autophagy flux protein P62. In a colon cancer xenograft model, a single intravenous injection of the drug combination significantly decreased tumor growth in comparison to the individual treatments. Most importantly, the combination treatment did not result in increased toxicity as assessed by body weight loss. The mechanism of combination treatment-induced cell death both *in vitro* and *in vivo* appeared to be apoptosis. Supportive of autophagy flux blockade as the underlying synergy mechanism, treatment with other autophagy maturation inhibitors, but not autophagy initiation inhibitors, were similarly synergistic with vinblastine. Additionally, knockout of the autophagy protein Beclin-1 suppressed combination treatment-induced apoptosis in vitro. In conclusion, *in vitro* and *in vivo* data support a synergistic antitumor activity of the nanoliposomal C6-ceramide and vinblastine combination, potentially mediated by an autophagic mechanism.

Keywords

combination therapy; autophagy; ceramide

Corresponding Author: Stephan T. Stern, Ph.D., DABT, Nanotechnology Characterization Laboratory, Advanced Technology Program, SAIC-Frederick, Frederick National Laboratory for Cancer Research, Frederick, Maryland 21702. Phone: 301-846-6198; Fax: 301-846-6399; sternstephan@mail.nih.gov.

Disclosure of Potential Conflicts of Interest: Penn State Research Foundation has licensed C6-ceramide nanoliposomal as well as C6-ceramide/vinblastine combinatorial nanoliposomal technologies to Keystone Nano, Inc. (State College, PA) for commercialization. Mark Kester is co-founder and Chief Medical Officer of Keystone Nano, Inc.. PAP, STS and SEM have US and international patent applications under review for ceramide and vinblastine combination therapy for cancer. The other authors have no conflicts to disclose.

1. Introduction

Many chemotherapeutics induce cancer cell apoptosis through mitochondrial or endoplasmic reticulum stress pathways [17]. Another pathway that has gained recent attention as a potential cancer drug target is the autophagy pathway. Autophagy, literally “self-eating”, is a survival pathway responsible for the breakdown of damaged organelles, protein aggregates, and long-lived proteins [19]. This process is initiated by double-membrane vacuoles, termed autophagosomes, engulfing these cellular components. Subsequently, fusion of autophagosomes with lysosomes results in the formation of single membrane autolysosomes in which the cellular contents are degraded by hydrolytic lysosomal enzymes [19].

Autophagy is known to play a role in both cancer suppression and survival depending on the stage of cancer development. From an evolutionary standpoint, autophagy (termed macroautophagy) is a survival mechanism whereby cellular proteins and organelles are recycled during periods of starvation in order to maintain cellular homeostasis. Similarly, tumors undergoing metabolic stress require autophagy. Once tumorigenesis is initiated, cancer cells in the progressive phase of the disease need a constant supply of nutrients to thrive. In solid tumors, however, these nutrients are deprived due to poor vascularization. Autophagy allows these tumor cells to survive under metabolic stress [8].

In addition to providing cellular building blocks necessary during times of nutrient deprivation, selective autophagy also functions to remove damaged organelles and proteins that can harm the cell and potentially cause disease, such as cancer. A role for autophagy as a tumor suppressor is supported by the fact that many cancers have a mono-allelic loss of *Beclin 1*, a gene required for the formation of autophagosomes [24]. In human breast, ovarian and prostate cancers, loss of *Beclin 1* gene function is associated with tumorigenesis [24, 34]. Haploinsufficient Beclin $1^{+/-}$mice, as well as mice deficient in the autophagy gene *Atg4C*, develop spontaneous tumors [29, 47]. Further confirming the role of autophagy genes in the suppression of tumorigenesis , loss of expression of other autophagy related genes , such as *Atg5*, Bax-interacting factor 1 (Bif-1), and ultraviolet radiation resistance-associated gene (UVRAG), have been identified in several human cancers [6, 13, 23]. Interestingly, defects in the autophagy pathway also appear to be involved in neurodegeneration, premature aging, muscular disease, and lysosomal storage disorders [21, 25, 28].

Currently, several agents that modulate autophagy are undergoing evaluation as cancer therapeutic agents [1]. In light of the dual role autophagy plays in cancer initiation and progression, there is an ongoing controversy surrounding whether the autophagy pathway primarily represents a pro-survival or pro-cell death mechanism with regard to cancer therapy [45]. The induction of autophagy by anti-cancer therapies (e.g., mTOR inhibitor rapamycin) could provide nutrients to proliferating cancer cells, or, conversely, initiate autophagic (type II programmed cell death) cell death. Alternatively, blockade of autophagy by agents that inhibit autophagy initiation (e.g., PI3K inhibitor 3-methyladenine (3-MA)) or autophagosome maturation/degradation inhibitors (e.g., lysosomotropic agent chloroquine) could block nutrient supply, effectively starving the cancer cells, or allow accumulation of damaged organelles, such as mitochondria, that could induce oxidative stress and further cancer progression. While the effect of autophagy modulating agents appears to be highly dependent upon the cancer being evaluated, it is interesting to note that agents which inhibit autophagosome maturation/degradation, as opposed to autophagy initiation, often have distinct effects on cancer cells when combined with an inducer of autophagy (chemotherapeutics or radiation) [22]. These autophagosome maturation/degradation inhibitors, such as the lysosomotropic agent hydroxychloroquine, block fusion of autophagosomes with lysosomes, preventing subsequent degradation of the autophagosomes

and resulting in futile autophagy cycling [22]. When combined with agents that induce autophagy in cancer cells, inhibitors of autophagy initiation (e.g., 3-MA), often antagonize cytotoxicity, while autophagosome maturation/degradation inhibitors synergistically increase cytotoxicity and induce apoptosis. For example, the autophagy initiation inhibitor 3-MA decreased the toxicity of temozolomide (TMZ), a known autophagy inducer, in glioma cells, while the autophagosome maturation/degradation inhibitor bafilomycin A1 potentiated TMZ cytotoxicity and induced apoptosis in the same cells [16]. Several studies have demonstrated that treatment of cancers with agents that induce autophagy in combination with agents that block autophagosome maturation/degradation result in synergistic apoptotic cell death. For example, co-treatment of hepatocellular carcinoma HepG3B and Huh7 xenografts with the autophagy inducer temosirolimus (mTOR inhibitor) and autophagy maturation/degradation inhibitor vinblastine (microtubule destabilizing agent) resulted in synergistic antitumor activity and decreased expression of anti-apoptotic proteins [49]. Similarly, another mTOR inhibitor and autophagy inducer, rapamycin, in combination with vinblastine synergistically suppressed growth, induced apoptosis, and increased survival in an orthotopic human neuroblastoma xenograft model [27].

The antitumor activity of short-chain cell-permeable ceramides (C2 and C6) has been demonstrated against various cancer cell lines in vitro and in vivo [7, 26, 40–42]. Ceramides are well-documented bioactive sphingolipid second-messengers involved in various cellular processes such as cell growth, differentiation, apoptosis, and autophagy [31]. It has been well established that ceramide treatment can induce autophagy by downregulating nutrient transporters, similar to the selective homeostatic response observed during nutrient deprivation [12]. With regard to the use of C6-ceramide as a therapeutic, systemic delivery of C6-ceramide is challenging due to its poor solubility. This has been overcome by incorporating C6-ceramide in the lipid bilayer of a nanoliposome [40]. Nanoliposomal C6-ceramide is soluble and the nanoliposome protects the ceramide from enzymatic degradation, increasing antitumor activity [41]. The C6-ceramide nanoliposomes are stable in biological fluids and nontoxic in animal [50].

Recent studies have demonstrated that vinblastine, a well-known microtubule-depolymerizing vinca alkaloid, disrupts autophagosome maturation/degradation by preventing movement of autophagosomes and their fusion with lysosomes [20, 46]. Acetylated microtubules, in particular, are critical for fusion of autophagosomes and lysosomes to form autolysosomes, and are selectively affected by vinblastine, unlike other microtubule toxins such as paclitaxel [46]. Consequently, vinblastine has been shown to be a powerful disruptor of autophagy flux in vitro and in vivo [2, 36]. While vinblastine is used clinically for acute leukemias and some solid tumors in combination with other chemotherapeutics, it is used marginally in hepatocellular carcinoma and colon cancer due to limited efficacy and toxicities (e.g., myelosuppression, nausea). Thus, improving the efficacy of vinblastine with ceramide combinatorial therapy offers new potential for this old drug. The human HepG2 and LS 174T cell lines were chosen as representative models of hepatocarcinoma and colon cancers, respectively. The present study evaluates the in vitro and in vivo effects of combination treatment with the autophagy inducer, C6-ceramide and the autophagosome maturation/degradation inhibitor vinblastine in multiple cancer models. To understand the synergistic cytotoxicity observed with combination treatment in the human hepatocarcinoma and colon cancer cell lines, we further evaluated autophagy disruption and apoptosis as potential mechanisms. In addition to these in vitro mechanistic studies, we also conducted an in vivo efficacy study in a human colon cancer xenograft utilizing a single systemic administration of the individual agents or their combination to confirm the in vivo relevance of the observed synergy. Data support the hypothesis that the nanoliposomal C6-ceramide-vinblastine combination therapy results in synergistic anti-cancer activity via blockade of pro-survival autophagy.

2. Materials and Methods

2.1 Materials

Vinblastine sulfate, protease inhibitor cocktail, phenylmethylsulphonyl fluoride (PMSF), methanol, Tween 20, Dulbecco's phosphate buffered saline (PBS), acetaminophen and cisplatin were purchased from Sigma (St. Louis, MO). 1,2-Dioleoyl-*sn*-glycero-3-phosphocholine, 1,2-dioleoyl-*sn*-glycero-3-phosphoethanolamine, *N*-hexanoyl-D-erythro-sphingosine (C6), 1,2-distearoyl-*sn*-glycero-3-phosphoethanolamine-*N*-[methoxy polyethylene glycol-2000], *N*-octanoyl-sphingosine-1-[succinyl(methoxy polyethylene glycol-750)] (PEG(750)-C_8), *N*-[6-[(7-nitro-2-1,3-benzoxadiazol-4-yl)amino]hexanoyl]-D-erythro-sphingosine (NBD-C_6), and *N,N*-dimethyl-D-erythro-sphingosine (DMSph) were purchased from Avanti Polar Lipids (Alabaster, AL*)*. Clinical grade Taxol (paclitaxel formulation) for in vitro experiments and vinblastine sulfate for animal studies were purchased from the NIH pharmacy. Cell extraction buffer, 4–20% Tris-Glycine gels, Tris-Glycine running buffer (10X), NuPAGE LDS 4X sample buffer, Tris-Glycine transfer buffer (25X), SeeBlue® Plus2 pre-stained standard, Hank's balanced salt solution (with calcium and magnesium) (HBSS), Lysotracker Red DND-99, and Celltracker Green CMFDA were purchased from Invitrogen (Carlsbad, CA). Blotting paper, Westran S, polyvinylidene fluoride (PVDF) protein blotting membrane, and Hyperfilm ECL were purchased from GE Healthcare/Whatman (Piscataway, New Jersey). Tris-buffered saline (TBS) (25X) was purchased from Amresco (Solon, OH). StartingBlock blocking buffer, ECL Western blotting substrate, BCA protein assay, fetal bovine serum (FBS), RPMI-1640 cell culture media (phenol-free), RPMI-1640 cell culture media (with phenol), and L-glutamine were purchased from Thermo Scientific/Pierce/Hyclone (Rockford, IL). Mouse monoclonal antibody (anti-LC3 antibody) was purchased from nanoTools USA (San Diego, CA). M199 Cell culture media was purchased from Cambrex (East Rutherford, NJ). Peroxidase-conjugated AffiniPure donkey anti-mouse IgG was purchased from Jackson ImmunoResearch Labs (West Grove, PA). Rabbit polyclonal antibody (SQSTM1/p62 antibody) was purchased from Cell Signaling Technology (Danvers, MA). Quick Start Bradford dye reagent (1X) was purchased from Bio-Rad (Hercules, CA). Caspase-3 fluorometric assay kit was purchased from BioVision, Inc. (Mountain View, California). Apo-ONE homogeneous caspase-3/7 assay kit was purchased from Promega (Madison, WI). All other chemicals and reagents were obtained from Fisher Chemical Co. (Fair Lawn, NJ) or one of the above suppliers, and all were of reagent grade or better.

2.2 Cell lines and culture conditions

The human hepatocarcinoma cell line (HepG2) and human colon cancer cell line (LS174T) were obtained from ATCC (Manassas, VA). Both cell lines were passaged for no more than 12 times, and not more than 3 months from initial stock plating. Species and organ authencity of the HepG2 and LS 174T cell lines were determined by the ATCC using COI assay and STR analysis, respectively. Both cell lines were cultured as monolayers in RPMI 1640 supplemented with 2 mM L-glutamine and 10% FBS, at 37°C in 5% CO_2.

2.3 Nanoliposomal formulation

PEGylated C6-ceramide (30 mol% ceramide) and ghost (no C6-ceramide) nanoliposomal formulations were prepared as described previously [41]. In brief, chloroform solubilized lipids were combined in a specific molar ratio [1,2-dioleoyl-*sn*-glycero-3-phosphocholine (DSPC)/1,2-dioleoyl-*sn*-glycero-3-phosphoethanolamine (DOPE)/1,2-distearoyl-*sn*-glycero-3-phosphoethanolamine-*N*-[methoxy PEG(2000)] (PEG2000-DSPC)/PEG(750)-C8-ceramide/C6-ceramide (3.75:1.75:0.75:0.75:3.0 molar ratio)] for the formulation of C6-ceramide containing nanoliposome; the ghost nanoliposome was prepared by combining DSPC, DOPE, and PEG2000-DSPC in a 5.66:2.87:1.47 molar ratio. The chloroform

solubilized lipids were then dried under a stream of nitrogen above the lipid transition temperatures for each lipid, and hydrated with sterile isotonic 0.9% NaCl solution. The resulting solution was sonicated for 2 minutes followed by extrusion through 100 nm polycarbonate membranes using an Avanti Mini Extruder (Avanti Polar Lipids, Alabaster, AL).

2.4 Hydrodynamic size determination

The hydrodynamic diameter of the nanoliposomes were measured using a Malvern Zetasizer Nano ZS instrument (Malvern Instruments, Southborough, MA) with a backscattering detector in batch mode at 25°C using a low volume quartz microcuvette. Stock solutions of C6-ceramide nanoliposomes and ghost nanoliposomes were diluted in saline to 1 mg/mL of total lipid (corresponding to 0.3 mM ceramide) concentration. Hydrodynamic size for nanoliposomes is reported as the intensity-weighted average. A total of 12 measurements per sample were made. Hydrodynamic diameters between different batches of nanoliposomes were analyzed to ensure consistent synthesis.

2.5 Zeta potential determination

Zeta potential of the ghost and C6-ceramide nanoliposomes were determined using a Malvern Zetasizer Nano ZS instrument at 25°C. Ghost- and C6-ceramide nanoliposomes were diluted to 1 mg/mL of total lipid (corresponding to 0.3 mM ceramide) concentration in 10 mM NaCl and the samples were loaded into folded capillary cells. An applied voltage of 100 V was used. The pH of the ghost- and C6-ceramide nanoliposomes was measured before and after zeta potential measurements. Three measurements were taken for each nanoliposomal samples. Zeta potential between different batches of nanoliposomes was analyzed to ensure consistent synthesis.

2.6 C6-Ceramide concentration determination

The C6-ceramide concentration in the nanoliposomes was determined by RP-HPLC. The chromatographic system consisted of a degasser (Agilent G1379A, Palo Alto, CA), capillary pump (Agilent G1378A), micro well-plate autosampler (Agilent G1377A), Zorbax 300SB-C18 column (1.0 mm ID × 150 mm, 3.5 μm, Agilent), and a diode array detector (Agilent G1315B). The mobile phase consisted of acetonitrile with 30% (v/v) water and methanol (HPLC grade, with 0.14% (w/v) trifluoroacetic acid) at a flow rate of 50 μL/min. The elution gradient was 20% methanol for 5 minutes, ramp to 40% methanol in 10 minutes, hold at 40% methanol for 5 minutes, and ramp down to 20% methanol in 5 minutes. Calibration standards of C6-ceramide (Avanti Polar Lipids; Alabaster, AL) were prepared at various concentrations ranging from 50 – 500 μg/mL in 20% methanol. Samples were prepared by lyophilizing 25 μL C6-ceramide liposomes and reconstituting in 360 μL of 20% methanol and 80% acetonitrile with 30% (v/v) water. Samples were vortexed and centrifuged, and the supernatant was analyzed via RP-HPLC. The sample volume injected was 5 μL and the ceramide analyte was detected at 205 nm. Samples were run in triplicate. C6-ceramide loading between different batches of nanoliposomes was analyzed to ensure consistency.

2.7 In vitro cytotoxicity assays

In vitro cytotoxicity in HepG2 and LS174T cells was performed using an MTT [32] or SRB cell viability [15] assay, respectively. In brief, HepG2 cells (5×10^4 cells/well) or LS174T cells (2×10^4 cells/well) were seeded into 96-well microtiter plates. Cells were pre-incubated for 24 h prior to drug treatment and were approximately 80% confluent. To obtain a concentration-response curve, cells were treated with varying concentrations of ghost nanoliposomes (volume equivalent to C6-ceramide nanoliposomes) and C6-ceramide nanoliposomes (1.4 – 360 μM of C6-ceramide for HepG2; 0.7 – 180 μM of C6-ceramide for

LS174T), serially diluted in cell culture media. Cells were treated with drug concentrations, media control (negative control) or 50 μM cisplatin (positive control) in the dark for 48 h, in triplicate. Cell viability in HepG2 cells was determined by the MTT assay with absorbance at 570 nm and a reference wavelength of 680 nm. Cell viability in LS174T cells was determined by the SRB assay with absorbance at 510 nm. Viability for both cell lines was expressed as percent media treated control.

To evaluate synergy, we performed C6-ceramide-vinblastine combination experiments in HepG2 and LS174T cell lines. Cells were treated with varying concentrations of vinblastine (0.0078 – 1 μM for HepG2; 10^{-12} – 100 μM for LS174T) alone, or in combination with ghost nanoliposomes (volume equivalent to C6-ceramide), or C6-ceramide nanoliposomes (12, 23, and 47 μM C6-ceramide for HepG2; 2.5, 5, and 10 μM C6-ceramide for LS174T) in cell culture media, and further incubated for 48 h. Cytotoxicity was assessed by the MTT assay for HepG2 cells and the SRB cell viability assay for LS174T cells. In addition, we performed C6-ceramide-chloroquine and C6-ceramide-paclitaxel combination experiments in the HepG2 cell line. Cells were treated with varying concentrations of chloroquine (1.6 μM – 200 μM) or paclitaxel (0.5 μM – 62.5 μM; Taxol formulation was used for in vitro studies due to poor solubilty of paclitaxel in cell culture media) alone, or in combination with ghost nanoliposomes (volume equivalent to C6-ceramide) or C6-ceramide nanoliposomes (23 μM C6-ceramide in combination with chloroquine; 12, 23, and 45 μM C6-ceramide in combination with paclitaxel) in cell culture media. Cytotoxicity was assessed by the MTT assay after 24 h for paclitaxel and 48 h for chloroquine treatments.

In order to determine the IC_{50} values, the MTT or SRB cytotoxicity assay 48 h concentration- response curves with eight vinblastine concentrations were analyzed by log-probit analysis (Finney method; BioStat Professional 5.8.4, AnalystSoft, Inc., Vancouver, Canada).

In order to evaluate the combination response in comparison to the individual agents, in vitro cytotoxicity data was analyzed by median effect analysis (as described elsewhere [5] to obtain a combination index (CI) value. The formula used for the CI analysis was:

$$\mathrm{CI} = [\mathrm{C_6 - Cer}]\,/\mathrm{IC}_{50}^{\mathrm{C6-Cer}} + [\mathrm{Vin}]\,/\mathrm{IC}_{50}^{\mathrm{Vin}}$$

CI values less than 1 indicate synergism, while CI values equal to 1 or greater than 1 indicate additive and antagonistic drug effects, respectively.

2.8 Caspase activation assay

Activation of the caspase 3 enzyme, a marker of caspase-dependent apoptosis, was measured by two different assays. The first assay normalized caspase 3 activity in cell lysates to total protein concentration, using the Caspase-3 fluorometric assay kit (BioVision, Inc., Mountain View, California), as described previously [33]. The total protein concentration was estimated by the Bradford protein assay kit. The second method utilized the Apo-One Homogeneous Caspase *3*/7 Assay kit (Promega, Madison, WI), a high throughput screening method to evaluate activation of caspase 3/7 enzymes. This method does not involve isolation of cell lysates, and the caspase 3/7 levels are not normalized to total protein. In an initial experiment, caspase 3 activation was evaluated in HepG2 cells. The cells were plated at 1.5×10^6 cells/well in 6-well plates and were allowed to grow for an additional 24 h, reaching an approximate 80% confluence. The cells were treated with C6-ceramide nanoliposomes alone at 11, 23, and 45 μM concentrations, or 25 mM acetaminophen (APAP; positive control), and caspase 3 enzyme activity was evaluated following incubation for 24 and 48 h. Caspase 3 enzyme activity was measured by

spectrophotometer at an excitation of 415 nm and emission at 505 nm, and normalized to total lysate protein, which was measured by Bradford assay at 595 nm absorbance. In the combination agent studies, apoptosis was monitored using the Apo-One Homogeneous caspase 3/7 assay kit. HepG2 cells were plated at 2×10^5 cells/well into 96-well plate format and were allowed to grow for an additional 24 h reaching an approximate 80% confluence. C6-ceramide nanoliposomes (12 or 24 μM*)* were co-treated in the presence of varying concentrations of vinblastine (0.004 – 1 μM*)*. Similarly, LS174T cells were plated at 4×10^4 cells/well into 96-well plate format and were allowed to grow for an additional 24 h, reaching an approximate 80% confluence. C6-ceramide nanoliposomes (24 μM) were co-treated in the presence of varying concentrations of vinblastine (0.004 – 1 μM). All treatments were performed in triplicate. Following incubation in the dark for 24 h at 37°C, cells were washed with media and incubated for an hour with kit reagents on a shaker (300–500 rpm). Caspase 3/7 enzyme activity was measured by spectrophotometer at an excitation of 499 nm and emission at 521 nm per vendor's instructions. Data are presented as percentage control caspase 3/7 activity.

2.9 Lysotracker Assay

The detailed protocol for this assay has been described previously [15]. Briefly, HepG2 cells were plated at 2×10^4 cells/well into 96-well microtiter plate format. Cells were treated with 24 μM C6-ceramide nanoliposomes in combination with varying concentrations of vinblastine (0.0078 – 1 μM) for 6, 24, and 48 h. Media was used as the negative control. Following incubation, cells were washed twice with cell culture media and incubated for an hour at 37°C in 100 μL of 50 nM Lysotracker Red DND-99 (Invitrogen Inc., Carlsbad, CA) and 10 μM Celltracker Green CMFDA (Invitrogen Inc., Carlsbad, CA) co-stain in phenol-free RPMI 1640 media, which stain lysosomes and viable cells, respectively. The cells were washed twice with 200 μL of phenol-free RPMI 1640 media. The plate fluorescence for Lysotracker Red and Celltracker Green was read at 544 nm/590 nm and 492 nm/517 nm, respectively. Lysotracker response was recorded as percent control response normalized to percent control Celltracker response.

2.10 Western blot

LC3 western blot analysis in HepG2 and LS17T cell lines was performed previously [39]. In brief, cells were treated with C6-ceramide nanoliposomes alone (47 μM for HepG2 cells; 12 μM for LS174T cells), 0.2 μM vinblastine alone, or in combination for 24 h. Media was used as the negative control and serum-starvation as the positive control. Total protein was isolated using Invitrogen Cell Extraction Buffer containing protease inhibitors (Sigma, St. Louis, MO). Total protein lysates (20 μg) from each treatment were loaded, separated on 4–20% tris-glycine SDS-PAGE gels, and transferred onto PVDF nylon membranes for immunoblotting.

The protein-transferred membrane was probed with primary antibody specific to anti-LC3 (1:200 dilution in StartingBlock blocking buffer) or anti-P62 (1:1000 dilution in 5% BSA blocking buffer) for 2 h at room temperature. The membrane was washed twice with tris-buffered saline containing 0.01%Tween-20 for 15 min each, followed by incubation with secondary donkey anti-mouse IgG-HRP conjugate (1:50,000 dilution in StartingBlock blocking buffer) for 1 h at room temperature. The membrane was then washed twice with tris-buffered saline containing 0.01% Tween-20 for 15 min each. The washed membrane was incubated with ECL peroxidase substrate solution and the immunoblot was developed using Hyperfilm ECL. The membrane was then incubated with stripping buffer followed by re-probing with antiβ-actin antibodies.

2.11 Autophagy analysis in mCherry-EGFP-LC3 transfected cells

HepG2 cells were stably transfected with the pBABE-puro-mCherry-EGFP-LC3B plasmid, a gift from Dr. Jayanta Debnath (Addgene plasmid #22418). The stably transfected HepG2 cells were plated onto 8-well chamber slides at a density of 2×10 cells/mL and incubated at 37°C for 24 h.

Each well was treated with media (negative control), 0.1 μM vinblastine, 12 μM C6-ceramide nanoliposomes, or 12 μM C6-ceramide nanoliposomes in combination with 0.1 μM vinblastine treatment and incubated at 37°C for 6 h. At an appropriate time point, media was aspirated and cells were washed twice with ice cold PBS. Cells were fixed with 4% formaldehyde and incubated at 4°C for 20 min. Following incubation, cells were washed with ice cold PBS and stored at 4°C. The slides were imaged using a Zeiss LSM NLO510 confocal microscope with 40x oil objective. The excitation wavelengths used for the GFP and mCherry were 488 nm and 543nm, respectively.

2.12 Short interfering RNA

SMARTpool siRNA targeting against Beclin-1, ON-TARGET pooled oligonucleotides (Cat # L-010552-00-0010), and scrambled siRNA (Cat # D-001810-10-05) duplexes were procured from Dharmacon RNAi Technologies. HepG2 cells were seeded at 20,000 cells/well (30–40% confluence) in 96-well plates and were transfected with varying concentrations of the siRNA using DharmaFECT 4 transfection reagent (Dharmacon RNAi Technologies) for 48 h. By Western blot analysis (as in section 2.10), protein lysates were prepared from the siRNA transfected cells and probed with Beclin-1 antibody (1:1000 dilution, Dharmacon RNAi Technologies) and the protein loading was normalized to β-actin.

For caspase 3/7 activity analysis, cells were transfected with 50, 100, or 200 nM mock (DharmaFECT 4), scrambled, and Beclin-1 specific siRNA for 48 h followed by treatment with 12 μM C6-ceramide nanoliposomes alone, 0.1 μM vinblastine alone, or combination treatment for 24 h. Apo-One Homogeneous Caspase 3/7 Assay kit (Promega, Madison, WI) was utilized to evaluate activation of caspase 3/7 enzymes.

2.13 Transmission electron microscopy

HepG2 cells were plated in 6-well chambers and allowed to grow for 24 h prior to initiation of treatment. Cells were treated for 24 h with complete media (negative control), C6-ceramide nanoliposomes alone (47 μM for HepG2 cells; 12 μM for LS174T cells), 0.2 μM vinblastine alone, or in combination, in duplicate. Following 24 h treatment, cells were washed twice with media prior to fixing (4% formaldehyde, 2% glutaraldehyde in 0.1 M sodium cacodylate buffer). Post-fixation staining of cells was performed in osmium tetroxide (1% osmium tetroxide in 0.1 M cacodylate buffer) and uranyl acetate (0.5% uranyl acetate in 0.1 M cacodylate buffer). Following the post-fixation staining step, cells were dehydrated stepwise in ethanol and embedded in embed-182 epoxy resin. Thin sections of 70–90 nm were trimmed using an ultramicrotome and were transferred onto formvar-copper mesh grids. Sections were then further stained with 3% uranyl acetate and lead citrate. Stained sections were carbon coated and imaged with a Hitachi H7600 microscope at 80 kV.

2.14 In vivo therapeutic efficacy of combination treatment

The in vivo efficacy of C6-ceramide nanoliposomes in combination with vinblastine was evaluated in a human colon cancer xenograft model (LS174T). Animals were acclimated to the study environment for two weeks prior to study initiation. Animal rooms were kept at 50% relative humidity, 68–72°F with 12 h light/dark cycles. Female athymic NCr-nu/nu mice 7 weeks-old were housed by treatment group, with 5 animals/cage, with ¼” corncob

bedding. Animals were allowed *ad libitum* access to Purina 18% NIH Block and chlorinated tap water. The Frederick National Laboratory for Cancer Research (FNLCR; formerly the National Cancer Institute at Frederick) is accredited by Association for Assessment and Accreditation of Laboratory Animal Care (AAALAC) International and follows the Public Health Service *Policy for the Care and Use of Laboratory Animals* (Health Research Extension Act of 1985, Public Law 99–158, 1986). Animal care was provided in accordance with the procedures outlined in the *Guide for Care and Use of Laboratory Animals* (National Research Council, 1996; National Academy Press, Washington, D.C.). All animal protocols were approved by the FNLCR institutional Animal Care and Use Committee. The experiments outlined herein are scientifically justified and do not represent an unnecessary duplication of previous work.

Tumor cells were inoculated into the left flank of 7 week-old female athymic nude mice (Charles River laboratories, Frederick, MD) by subcutaneous injection of 6×10^6 LS174T cells in 0.1 mL Hanks Balanced Salt Solution. Tumors were allowed to grow for 7 days post-implantation, or until tumors reached approximately 5 mm in longest diameter, at which time chemotherapy treatment was initiated. Animals were randomly assigned to saline vehicle or treatment groups. Each dosing group consisted of five animals with flank tumors. Treatment groups were 20 mg/kg of the clinical formulation of vinblastine (vinblastine sulfate) administered in 20 mL/kg dosing volume, 20 mg C6-ceramide/kg of the nanoliposomal formulation administered in 5 mL/kg dosing volume, combination treatment with C6-ceramide and vinblastine, or equivalent volumes of ghost nanoliposome or saline controls. Study drugs were given as single doses by intravenous tail vein injection, with vinblastine dosed 15 min post nanoliposome dose for combination treatments. Animals were monitored daily for mortality and signs of pharmacologic or toxicologic effects. Body weights and tumor growth were measured on alternate days until the study was terminated on study day 29.

Tumor measurement for each mouse was recorded using vernier calipers, and tumor volumes were calculated according to the formula: $(\text{width}^2 \times \text{length})/2$ (in mm^3), where width is always the smaller of the two caliper measurements. The neoplasia-related endpoint criteria were ulcerated tumor and tumor diameter ≥2 cm, at which point animals were euthanized. The morbidity criteria for euthanization included loss of greater than 20% of initial body weight and immobility. All surviving animals were euthanized at study termination on day 29 and necropsy, consisting of tumor sizing, organ weight measurement, gross organ description, hematology and clinical chemistry, and histopathology of all organs identified with gross lesions, was performed.

In addition, the LS174T colon cancer model was used to evaluate the induction of apoptosis by the combination treatment in comparison to single agent as described above. Each dosing group consisted of three animals with flank tumors. Treatment groups were 15 mg/kg of the clinical formulation of vinblastine (vinblastine sulfate) administered in 15 mL/kg dosing volume, 45 mg C6-ceramide/kg of the nanoliposomal formulation administered in 15 mL/kg dosing volume, combination treatment with C6-ceramide and vinblastine, or equivalent volumes of ghost nanoliposome or saline controls. Study drugs were given as single doses by intravenous tail vein injection, with vinblastine dosed 15 min post nanoliposome dose for combination treatments. Animals were euthanized after 72 h post treatment and resected tumors were fixed for the analysis of apoptosis by deoxynucleotidyl transferase-mediated nick end-labeling (TUNEL) using a commercial kit (Millipore S7100 Apoptag Peroxidase In-situ Apoptosis Detection Kit).

2.15 Statistical analysis

Statistical differences were determined using Student's T Test and ANOVA, with post-hoc comparisons by Duncan's test using Statistica version 7.1 software (StatSoft Inc, Tulsa, OK).

3.0 Results

3.1 Physicochemical characteristics of nanoliposomes

The hydrodynamic diameters and zeta potentials of ghost- and C6-ceramide nanoliposomes were measured in saline and 10 mM NaCl, respectively, using dynamic light scattering at 25°C. The intensity weighted hydrodynamic diameter of ghost- and C6-ceramide nanoliposomes in saline were 88 nm and 89 nm, respectively (Supplementary Fig. S1A; Supplementary Table S1). Both nanoliposomes had neutral zeta potentials due to the presence of the hydrophilic PEG coating (Supplementary data Fig. S1B). Zeta potential values ±10 mV are generally considered neutral. By HPLC analysis, the concentration of C6-ceramide in the nanoliposomes was determined to be 2 mg C6-ceramide/mL (Supplementary Fig. S2).

3.2 Cytotoxicity and apoptotic activity of C6-ceramide nanoliposome in HepG2 cells

In an initial in vitro cytotoxicity experiment, nanoliposomal C6-ceramide treatment resulted in a greater concentration-dependent decrease in HepG2 cell viability compared to treatment with the ghost nanoliposomal formulation (formulation with no drug) (Fig. 1A). The calculated 48 h IC50 value from the dose-response curve for nanoliposomal C6-ceramide was 51 μM (Supplementary Table S2).

Based on initial in vitro cytotoxicity results, nanoliposomal C6-ceramide was tested at three different concentrations (11, 23, and 45 μM of C6-ceramide), up to the calculated 48 h IC_{50}, for the activation of caspase 3, a marker for apoptosis (Fig. 1B). C6-ceramide nanoliposome treatment did not significantly increase the activation of caspase 3 in comparison to the media control.

3.3 Nanoliposomal C6-ceramide in combination with vinblastine synergistically enhances in vitro cytotoxicit

The in vitro cytotoxicity of nanoliposomal C6-ceramide (an established autophagy inducer) [12] in combination with vinblastine (a known autophagosome maturation/degradation inhibitor) [46] was evaluated in HepG2 and LS174T cells. The concentrations of C6-ceramide evaluated were 12, 23, and 47 μM for HepG2 cells; 2.5, 5.0, and 10 μM for LS174T cells. In combination with non-toxic concentrations of vinblastine, between 7.8×10^{-3} - 1 μM for HepG2 and 10^{-12} – 10^{2} μM for LS174T cells, all three concentrations of the C6-ceramide nanoliposomes synergistically decreased the cell viability of the HepG2 (Fig. 2A) and LS174T cells (Fig. 2C) at 48 h as measured by the MTT or SRB cell viability assay, respectively. Treatment of HepG2 and LS174T cells with ghost nanoliposome in combination with vinblastine, however, did not increase cell death (Figs. 2B and 2D). IC50 values were estimated based on the concentration-response of ghost or C6-ceramide nanoliposomes in combination with vinblastine in HepG2 and LS174T cells (Supplementary Table S2). In addition, there was a synergistic decrease in HepG2 cell viablity when treated with chloroquine, a known autophagosome maturation/degradation inhibitor, in combination with C6-ceramide nanoliposomes at 48 h (Supplementary Fig. S3A). Chloroquine in combination with ghost nanoliposomes did not affect cell viability. By contrast, synergy was not observed with a C6-ceramide-paclitaxel combination treatment (Supplementary Fig. S3B).

The combination index (CI) analysis was used to determine an additive or synergistic response to the combination treatment. Based on the 48 h cytotoxicity analysis, CI values for the combination treatment were 0.24 and 0.47 in the HepG2 cell line, indicating a synergistic increase in cell death (Supplementary Table S2). Similar CI values were obtained in LS174T cells also supporting synergism (Supplementary Table S2). The CI value for C6-ceramide-chloroquine combination treatment was 0.7, indicating a synergistic increase in cell death. On the contrary, based on 24 h cell viability analysis, synergy was not observed for the C6-ceramide-paclitaxel treatment (CI = 1.4).

3.4 Combination treatment results in blockade of autophagosome maturation/degradation

To determine if the synergy observed with combination treatment was indeed associated with autophagy blockade, cells were evaluated for Lysotracker Red dye uptake, expression of the autophagy marker microtubule associated protein light chain 3 (LC3) and autophagy flux marker P62. Accumulation of autophagic vacuoles, indicative of autophagy blockade, was also assessed by transmission electron microscopy.

The Lysotracker Red dye uptake assay was performed using HepG2 cells. HepG2 cells were treated with 24 μM of C6-ceramide nanoliposome in combination with varying concentrations of vinblastine, for 6, 24, or 48 h time periods. Following treatment, the cells were stained with Lysotracker Red dye and Celltracker Green dye, which are selectively taken up by the acidic lysosomes and viable cells, respectively. The Lysotracker Red fluorescence was normalized to Celltracker Green fluorescence to account for viable cells and expressed as percent control (Fig. 3A). The combination treatment resulted in a maximum value of over 200% control at 24 and 48 h.

Autophagy was further evaluated by an immunoblot analysis for LC3-II. During the formation of the double membrane autophagosome, cytosolic LC3-I is cleaved and lipidated to form LC3-II, which is then recruited to the early phagophore membrane, making LC3-II an excellent marker for autophagosomes. The cell lysates isolated from cells treated with the C6-ceramide nanoliposome and vinblastine combination showed a synergistic increase in the levels of LC3-II compared to either of the agents alone (Fig. 3B). P62 protein is a marker for autophagic flux, as the autophagy pathway normally degrades this protein. In agreement with the autophagy blockade hypothesis, degradation of P62 protein was not found in response to the combination treatment. This, taken together with the synergistic increases in LC3-II, is indicative of a blockade of autophagosome degradation.

In addition to the Lysotracker Red dye uptake assay and LC3-II protein analysis in HepG2 cells, the accumulation of autophagic vacuoles was also assessed by transmission electron microscopy. Electron microscopy is considered the gold standard for evaluating ultrastructural features of cells undergoing autophagy. Combination treatment resulted in a significant increase in autophagic vacuoles (autophagosomes, and early and late stage autolysosomes) in comparison to either of the treatments alone or media control (Fig. 3C). In addition to these results from the HepG2 cell line, we observed similar trends in autophagy markers LC3-II and P62, as well as autophagic vacuoles in response to combination treatment of LS174T cells (Supplementary data Fig. S4).

We further clarified the proposed blockade hypothesis of autophagy flux by utilizing the dual tagged mCherry-GFP-LC3 reporter construct, which allows simultaneous monitoring of autophagy induction and maturation/degradation. Treatment of stably transfected HepG2 cells with C6-ceramide resulted in increased red fluorescent puncta at 6 h suggesting the fusion of autophagosomes to lysosomes (mCherry-positive and GFP-negative; Fig. 3D). Vinblastine alone resulted in fewer colocalized GFP-positive and mCherry-positive fluorescent puncta (yellow), suggesting blockade of autophagosome degradation by the

treatment (Fig. 3D). We observed increased colocalization of GFP-positive and mCherry-positive fluorescent (yellow) in cells treated with C6-ceramide in combination with vinblastine. Enhanced accumulation of colocalized puncta confirms the inhibition of autophagosome degradation by vinblastine (Fig.3D).

3.5 Combination treatment increases caspase 3/7 activity

Caspase 3/7 activity, a marker of caspase-dependent apoptosis, was analyzed to evaluate whether the blockade of autophagy flux by co-treatment of C6-ceramide and vinblastine resulted in enhanced apoptotic cell death. Indeed, co-treatment of C6-ceramide nanoliposome (12 and 24 μM for HepG2; 24 μM for LS174T) and vinblastine in both HepG2 and LS174T cell lines led to a dramatic increase in caspase 3/7 activity as compared to the vinblastine treatment alone at 24 h (Fig. 4; Supplementary Fig. S5). As the apoptosis assay did not normalize to viable cell number, the decrease in caspase 3/7 activity at higher concentrations of vinblastine is likely due to a decreased number of viable cells contributing to caspase 3/7 activity (Fig. 4). These results suggest that C6-ceramide synergistically enhanced vinblastine-induced caspase-dependent apoptosis in HepG2 and LS174T cells.

3.6 Knockdown of Beclin-1 abrogates combination treatment induced caspase 3/7 activity

Beclin-1 is one of the key proteins required for the formation of the autophagosome [24]. We employed Beclin-1 knockdown to further clarify the autophagy-mediated cell death by combination treatment in HepG2 cells. By immunoblot analysis, we confirmed that Beclin-1 siRNA transfection for 48 h resulted in knockdown of Beclin-1 protein expression (Fig. S6). Transfection of HepG2 cells with scrambled siRNA did not affect Beclin-1 protein levels, which was similar to untransfected cells (data not shown). No decrease in cell viability was observed at the tested siRNA concentrations (data not shown). Inhibition of autophagy induction by Beclin-1 siRNA resulted in decreased caspase 3/7 activation by combination treatment, which was statistically significant in comparison to scrambled siRNA treated with combination agents (Fig. S6). In addition, an increase in caspase 3/7 activation was observed in C6-ceramide treated Beclin-1 siRNA transfected cells, suggesting inhibition of autophagy induction upon C6-ceramide treatment also results in increased apoptosis of cancer cells, but to a lesser degree than inhibition of autophagy maturation.

3.7 C6-ceramide synergistically enhances vinblastine antitumor activity

To explore if the synergy observed in vitro could be reproduced in vivo, an in vivo efficacy experiment was conducted in female nude mice with subcutaneously implanted LS174T human colon cancer cells. Combination treatment with a single intravenous injection of C6-ceramide nanoliposomes followed by vinblastine 15 min later resulted in a statistically significant suppression of tumor growth in comparison to vinblastine and C6-ceramide nanoliposome alone (Fig. 5A). Single dose treatment with either ghost or C6-ceramide nanoliposomes alone was ineffective and comparable to saline treatment. Administration of vinblastine alone resulted in an initial decrease in body weight, which was not exacerbated when the vinblastine was combined with C6-ceramide (Fig. 5B). In addition, organ weight, hematology, and clinical chemistry data provided no evidence of increased toxicity for the combination treatment over vinblastine treatment alone (data not shown). Animals euthanized from the study were either due to tumor diameter greater than 2 cm or tumor ulceration.

In order to evaluate apoptotic response to combination treatment, tumors were harvested 72 h post treatment for TUNEL staining. Combination treatment increased TUNEL staining in the tumors in comparison to single or control treatments (Fig. 5C). The synergistic increase in apoptotic activity by combination treatment in tumors corresponded with the enhanced

cell death and caspase 3/7 activity observed under in vitro conditions, suggestive of a common apoptotic cell death mechanism.

4.0 Discussion

In the present study, combination treatment with the autophagy inducer nanoliposomal C6-ceramide and autophagy maturation/degradation inhibitor vinblastine resulted in a synergistic increase in cytotoxic potency and apoptosis in human hepatocarcinoma (HepG2) and colon cancer (LS174T) cell lines. These data were further supported by in vivo findings demonstrating synergistic tumor growth suppression and increased TUNEL staining indicative of enhanced apoptosis by the drug combination in the LS174T xenograft. A single tail-vein administration of nanoliposomal C6-ceramide in combination with vinblastine in the LS174T tumor model resulted in prolonged inhibition of tumor growth over a two-week period without exacerbation of animal weight loss in comparison to vinblastine alone. Autophagy blockade was examined as a potential mechanism underlying the synergistic enhancement of anticancer activity by C6-ceramide-vinblastine combination treatment.

Systemic delivery of nanoliposomal C6-ceramide has been shown to have antitumor activity in various tumor models [26, 41, 42]. Encouragingly, the efficacy seen with our single dose combinatorial therapy in the LS174T nude mouse model is as good or even better than every other day dosing of C6-ceramide alone in breast cancer [41] or hepatocellular carcinoma [42] in vivo models. The primary mechanism proposed in these previous studies has been a pro-apoptotic mechanism. For example, C6-ceramide has been shown to decrease cell viability by diminution of AKT phosphorylation, which is a key kinase involved in pro-survival cell signaling, resulting in apoptotic cell death [42]. Several studies in the literature have also reported a pronounced increase in cytotoxic potency when C6-ceramide has been combined with doxorubicin [14] and paclitaxel [43], with enhanced apoptotic signaling suggested as a common mechanism underlying the therapeutic action of these C6-ceramide drug combinations.

Currently, there is significant interest in targeting the autophagy pathway to improve anticancer therapy and overcome multidrug resistance. Cancer cells may evade anticancer therapy by inducing autophagy, a survival response, and blocking the autophagy pathway has been shown to improve therapeutic response in some cases [1]. The lysosomotropic autophagosome maturation/degradation inhibitors chloroquine and hydroxychloroquine have been shown to sensitize various cancer cells to the cytotoxic effects of anticancer agents and ionizing radiation [38]. Based on encouraging preclinical studies, hydroxychloroquine is currently being evaluated in several clinical trials in combination with standard-of-care treatment regimens for a variety of cancers [1,11].

The present results are in agreement with findings from other researchers demonstrating that autophagy blockade can sensitize cancer cells to autophagy inducing chemotherapeutics through an apoptotic cell death mechanism [35, 37]. Previous studies have shown induction of autophagy by ceramides, which is suggested to be a homeostatic response resulting from down regulation of nutrient transporter proteins [12]. Consistent with the previous studies, ceramide-induced cytotoxicity is also synergistically enhanced by combination treatment with the autophagosome maturation/degradation inhibitor chloroquine [12]. To support the involvement of autophagy blockade as a mechanism involved in the therapeutic response of the C6-ceramide-vinblastine drug combination, LC3 levels, Lysotracker Red dye uptake, mCherry-GFP-LC3 fluorescent analysis, and accumulation of autophagic vacuoles by electron microscopy were evaluated. Indeed, C6-ceramide in combination with vinblastine treatment increased the levels of autophagic marker LC3-II, suggesting increased conversion of LC3-I to LC3-II and/or impaired clearance of autophagic vacuoles. Increased LC3-II

levels correlated with increased Lysotracker Red dye uptake, consistent with an accumulation of autolysosomal vacuoles. The an accumulation of autophagic vacuoles was confirmed by EM for the combination treatment in comparison to individual treatments.

Under homeostatic conditions, a balance exists between autophagosome formation and degradation, termed autophagic flux. Autophagic flux requires initial autophagosome formation followed by maturation of the autophagosome in a sequential process: 1) vesicular transport of autophagosomes to lysosomes; 2) autolysosome formation by organelle fusion; 3) and finally, degradation of the autolysosome contents (Fig. 6) [3]. Vinblastine, a microtubule-depolymerizing agent, disrupts cytoskeleton-mediated transport of vesicles and impairs the fusion of autophagosomes with lysosomes, blocking autophagosome maturation and degradation, and, thereby, autophagy flux [20]. For example, treatment of neuronal cells with vinblastine resulted in massive accumulation of autophagic vacuoles, similar to what is observed in neurodegenerative diseases [3]. In the present studies, the increase in LC3-II protein in response to the combination treatment, combined with lack of P62 protein diminution, is consistent with a blockade in autophagosome maturation.To further investigate autophagy flux, we transfected Hep G2 cells with dual tagged mCherry-GFP-LC3. Since the GFP green fluorescence is quenched by lysosomal acidic pH and mCherry red fluorescence is stable, red fluorescent puncta identify autolysosome and dual fluorescent puncta identify autophagosome. We observed increased GFP-negative/mCherry-positive puncta in C6-ceramide treated cells, confirming the induction of autophagy and increased formation of autolysosomes. By contrast, the increased colocalization of mCherry-positive/GFP-positive puncta observed in the combination treated cells supports disruption of autophagy flux.

The question remains how dysregulation of the autophagy pathway could result in apoptotic cell death. From the literature, it is evident that the apoptosis and autophagy pathways share several key signaling components and several opportunities for crosstalk exist [18, 30, 48]. One possible mechanisms of crosstalk is regulation of caspase-8 and −3 activation by the autophagy proteins Beclin 1 and LC3B, which are required for the induction of apoptosis by cigarette smoke extract (CSE) in human bronchial epithelial cells (Beas-2b) [18]. SiRNA knockdown of Beclin 1 and LC3B significantly inhibited the apoptotic response stimulated by CSE, suggesting an important role for these autophagy proteins in the interrelationship between the two pathways. In the present study, Beclin 1 knockdown by siRNA also resulted in a significant decrease in apoptosis in response to combination treatment, as measured by caspase 3/7 activitation. Another mechanism of crosstalk between the two pathways is via JNK1 -mediated phosphorylation of Bcl-2 [44]. For example, short-term nutrient starvation (4 h) in Hela cells induced JNK1-mediated phosphorylation of Bcl-2, leading to the dissociation of Beclin 1 from the Bcl-2 complex and resulting in initiation of autophagy. Following sustained activation of JNK1 in response to prolonged nutrient deprivation (16 h), Bax (a pro-apoptotic protein) was eventually released from the phosphorylated Bcl-2 complex, promoting apoptosis. These data suggest phosphorylation of Bcl-2 by JNK1 may act as a key switch in selecting between pro-survival (autophagy) and pro-death (apoptosis) responses. Interestingly, both ceramide and vinblastine have been shown to activate JNK-1 -mediated BCL-2 phosphorylation [4, 10, 30].

A recent report has suggested that vinblastine blockade of autophagosome maturation/degradation is mediated by depolymerization of acetylated microtubules [46]. In contrast, the microtubule stabilizing agent paclitaxel does not affect acetylated microtubules, does not block the autophagosome maturation/degradation step [46], and resulted in a less-than additive cytotoxic response when combined with C6-ceramide in HepG2 cells (Supplementary Fig. S3B). Since paclitaxel is an inhibitor of autophagy initiation [46], but not autophagosome maturation/degradation, this would suggest that blockade of

autophagosome maturation/degradation is crucial for synergy with C6-ceramide, rather than simply disruption of autophagy. This is similar to a study with the autophagy inducer TMZ, in which the inhibitor of autophagy initiation, 3-MA, did not improve drug efficacy, while the inhibitor of autophagosome maturation/degradation, bafilomycin A1, was very effective [16]. A similar synergistic enhancement of cytotoxicity and in vivo tumor growth suppression was observed in PTEN-null PC3 prostate cancer models, by the simultaneous knockdown of the autophagy suppressor Akt and treatment with the autophagosome maturation/degradation inhibitors chloroquine or bafilomycin A1[9]. Consistent with our findings, the autophagy initiation inhibitor 3-MA was ineffective in comparison to chloroquine in enhancing PC3 cytotoxicity induced by Akt knockdown, and actually antagonized chloroquine synergy. Cumulatively, these data and ours provide a rationale for therapeutic intervention in cancer whereby the initiation and maturation steps of the autophagy pathway are simultaneously targeted.

In conclusion, these results support the hypothesis that nanoliposomal C6-ceramide in combination with vinblastine enhances antitumor activity by targeting the autophagy pathway, via bloackade of pro-survival autophagy. Future studies will optimize dosing, investigate the underlying signaling mechanisms responsible for combination treatment synergy, and further clarify the importance of autophagy dysfunction in this process.

Supplementary Material

Refer to Web version on PubMed Central for supplementary material.

Acknowledgments

The authors wish to thank (all from SAIC-Frederick, Inc.) David Parmiter, Christina Burks, and Ulrich Baxa for TEM analysis, Diana Haines for TUNEL staining of tumor sections, and Rachael M. Crist for assistance with the preparation of the manuscript.

Financial Support: This project has been funded in whole or in part with federal funds from the National Cancer Institute, National Institutes of Health, under contract HHSN261200800001E. The content of this publication does not necessarily reflect the views or policies of the Department of Health and Human Services, nor does mention of trade names, commercial products, or organizations imply endorsement by the U.S. Government. The project was also funded, in part (MK), through support from the Ebberly Fund of Penn State College of Medicine.

References

1. Amaravadi RK, Lippincott-Schwartz J, Yin XM, Weiss WA, Takebe N, Timmer W, DiPaola RS, Lotze MT, White E. Principles and current strategies for targeting autophagy for cancer treatment. Clin Cancer Res. 2011; 17:654–666. [PubMed: 21325294]
2. Berkenstam A, Ahlberg J, Glaumann H. Isolation and characterization of autophagic vacuoles from rat kidney cortex. Virchows Arch B Cell Pathol Incl Mol Pathol. 1983; 44:275–286. [PubMed: 6141661]
3. Boland B, Kumar A, Lee S, Platt FM, Wegiel J, Yu WH, Nixon RA. Autophagy induction and autophagosome clearance in neurons: relationship to autophagic pathology in Alzheimer's disease. J Neurosci. 2008; 28:6926–6937. [PubMed: 18596167]
4. Bourbon NA, Yun J, Kester M. Ceramide directly activates protein kinase C zeta to regulate a stress-activated protein kinase signaling complex. J Biol Chem. 2000; 275:35617–35623. [PubMed: 10962008]
5. Chou TC, Talalay P. Quantitative analysis of dose-effect relationships: the combined effects of multiple drugs or enzyme inhibitors. Adv Enzyme Regul. 1984; 22:27–55. [PubMed: 6382953]
6. Coppola D, Khalil F, Eschrich SA, Boulware D, Yeatman T, Wang HG. Down-regulation of Bax-interacting factor-1 in colorectal adenocarcinoma. Cancer. 2008; 113:2665–2670. [PubMed: 18833585]

7. Daido S, Kanzawa T, Yamamoto A, Takeuchi H, Kondo Y, Kondo S. Pivotal role of the cell death factor BNIP3 in ceramide-induced autophagic cell death in malignant glioma cells. Cancer Res. 2004; 64:4286–4293. [PubMed: 15205343]
8. Degenhardt K, Mathew R, Beaudoin B, Bray K, Anderson D, Chen G, Mukherjee C, Shi Y, Gelinas C, Fan Y, Nelson DA, Jin S, White E. Autophagy promotes tumor cell survival restricts necrosis, inflammation and tumorigenesis. Cancer Cell. 2006; 10:51–64. [PubMed: 16843265]
9. Degtyarev M, De Maziere A, Orr C, Lin J, Lee BB, Tien JY, Prior WW, van Dijk S, Wu H, Gray DC, Davis DP, Stern HM, Murray LJ, Hoeflich KP, Klumperman J, Friedman LS, Lin K. Akt inhibition promotes autophagy and sensitizes PTEN-null tumors to lysosomotropic agents. J Cell Biol. 2008; 183:101–116. [PubMed: 18838554]
10. Fan M, Goodwin M, Vu T, Brantley-Finley C, Gaarde WA, Chambers TC. Vinblastine-induced phosphorylation of Bcl-2 and Bcl-XL is mediated by JNK and occurs in parallel with inactivation of the Raf-1/MEK/ERK cascade. J Biol Chem. 2000; 275:29980–29985. [PubMed: 10913135]
11. Garcia-Ma S, Alcaide A, Dominguez C. Pharmacological Control of Autophagy: Therapeutic Perspectives in Inflammatory Bowel Disease and Colorectal Cancer. Curr Pharm Des. 2012
12. Guenther GG, Peralta ER, Rosales KR, Wong SY, Siskind LJ, Edinger AL. Ceramide starves cells to death by downregulating nutrient transporter proteins. Proc Natl Acad Sci U S A. 2008; 105:17402–17407. [PubMed: 18981422]
13. Iqbal J, Kucuk C, Deleeuw RJ, Srivastava G, Tam W, Geng H, Klinkebiel D, Christman JK, Patel K, Cao K, Shen L, Dybkaer K, Tsui IF, Ali H, Shimizu N, Au WY, Lam WL, Chan WC. Genomic analyses reveal global functional alterations that promote tumor growth and novel tumor suppressor genes in natural killer-cell malignancies. Leukemia. 2009; 23:1139–1151. [PubMed: 19194464]
14. Ji C, Yang B, Yang YL, He SH, Miao DS, He L, Bi ZG. Exogenous cell-permeable C6 ceramide sensitizes multiple cancer cell lines to Doxorubicin-induced apoptosis by promoting AMPK activation and mTORC1 inhibition. Oncogene. 2010; 29:6557–6568. [PubMed: 20802518]
15. Johnson-Lyles DN, Peifley K, Lockett S, Neun BW, Hansen M, Clogston J, Stern ST, McNeil SE. Fullerenol cytotoxicity in kidney cells is associated with cytoskeleton disruption autophagic vacuole accumulation and mitochondrial dysfunction. Toxicol Appl Pharmacol. 2010; 248:249–258. [PubMed: 20713077]
16. Kanzawa T, Germano IM, Komata T, Ito H, Kondo Y, Kondo S. Role of autophagy in temozolomide-induced cytotoxicity for malignant glioma cells. Cell Death Differ. 2004; 11:448–457. [PubMed: 14713959]
17. Karmakar S, Choudhury SR, Banik NL, Ray SK. Induction of Mitochondrial Pathways and Endoplasmic Reticulum Stress for Increasing Apoptosis in Ectopic and Orthotopic Neuroblastoma Xenografts. J Cancer Ther. 2011; 2:77–90. [PubMed: 22468231]
18. Kim HP, Wang X, Chen ZH, Lee SJ, Huang MH, Wang Y, Ryter SW, Choi AM. Autophagic proteins regulate cigarette smoke-induced apoptosis: protective role of heme oxygenase-1. Autophagy. 2008; 4:887–895. [PubMed: 18769149]
19. Klionsky DJ. Autophagy: from phenomenology to molecular understanding in less than a decade. Nat Rev Mol Cell Biol. 2007; 8:931–937. [PubMed: 17712358]
20. Kochl R, Hu XW, Chan EY, Tooze SA. Microtubules facilitate autophagosome formation and fusion of autophagosomes with endosomes. Traffic. 2006; 7:129–145. [PubMed: 16420522]
21. Komatsu M, Waguri S, Chiba T, Murata S, Iwata J, Tanida I, Ueno T, Koike M, Uchiyama Y, Kominami E, Tanaka K. Loss of autophagy in the central nervous system causes neurodegeneration in mice. Nature. 2006; 441:880–884. [PubMed: 16625205]
22. Kondo Y, Kanzawa T, Sawaya R, Kondo S. The role of autophagy in cancer development and response to therapy. Nat Rev Cancer. 2005; 5:726–734. [PubMed: 16148885]
23. Liang C, Feng P, Ku B, Dotan I, Canaani D, Oh BH, Jung JU. Autophagic and tumour suppressor activity of a novel Beclin1-binding protein UVRAG. Nat Cell Biol. 2006; 8:688–699. [PubMed: 16799551]
24. Liang XH, Jackson S, Seaman M, Brown K, Kempkes B, Hibshoosh H, Levine B. Induction of autophagy and inhibition of tumorigenesis by beclin 1. Nature. 1999; 402:672–676. [PubMed: 10604474]

25. Lieberman AP, Puertollano R, Raben N, Slaugenhaupt S, Walkley SU, Ballabio A. Autophagy in lysosomal storage disorders. Autophagy. 2012; 8:719–730. [PubMed: 22647656]
26. Liu X, Ryland L, Yang J, Liao A, Aliaga C, Watts R, Tan SF, Kaiser J, Shanmugavelandy SS, Rogers A, Loughran K, Petersen B, Yuen J, Meng F, Baab KT, Jarbadan NR, Broeg K, Zhang R, Liao J, Sayers TJ, Kester M, Loughran TP Jr. Targeting of survivin by nanoliposomal ceramide induces complete remission in a rat model of NK- LGL leukemia. Blood. 2010; 116:4192–4201. [PubMed: 20671121]
27. Marimpietri D, Brignole C, Nico B, Pastorino F, Pezzolo A, Piccardi F, Cilli M, Di Paolo D, Pagnan G, Longo L, Perri P, Ribatti D, Ponzoni M. Combined therapeutic effects of vinblastine rapamycin on human neuroblastoma growth apoptosis and angiogenesis. Clin Cancer Res. 2007; 13:3977–3988. [PubMed: 17606732]
28. Marino G, Fernandez AF, Lopez-Otin C. Autophagy and aging: lessons from progeria models. Adv Exp Med Biol. 2010; 694:61–68. [PubMed: 20886757]
29. Marino G, Salvador-Montoliu N, Fueyo A, Knecht E, Mizushima N, Lopez-Otin C. Tissue-specific autophagy alterations and increased tumorigenesis in mice deficient in Atg4C/autophagin-3. J Biol Chem. 2007; 282:18573–18583. [PubMed: 17442669]
30. Pattingre S, Bauvy C, Carpentier S, Levade T, Levine B, Codogno P. Role of JNK1-dependent Bcl-2 phosphorylation in ceramide-induced macroautophagy. J Biol Chem. 2009; 284:2719–2728. [PubMed: 19029119]
31. Ponnusamy S, Meyers-Needham M, Senkal CE, Saddoughi SA, Sentelle D, Selvam SP, Salas A, Ogretmen B. Sphingolipids and cancer: ceramide and sphingosine-1- phosphate in the regulation of cell death and drug resistance. Future Oncol. 2010; 6:1603–1624. [PubMed: 21062159]
32. Potter TM, Stern ST. Evaluation of cytotoxicity of nanoparticulate materials in porcine kidney cells and human hepatocarcinoma cells. Methods Mol Biol. 2011; 697:157–165. [PubMed: 21116964]
33. Potter TM, Stern ST. Monitoring nanoparticle-treated hepatocarcinoma cells for apoptosis. Methods Mol Biol. 2011; 697:167–172. [PubMed: 21116965]
34. Qu X, Yu J, Bhagat G, Furuya N, Hibshoosh H, Troxel A, Rosen J, Eskelinen EL, Mizushima N, Ohsumi Y, Cattoretti G, Levine B. Promotion of tumorigenesis by heterozygous disruption of the beclin 1 autophagy gene. J Clin Invest. 2003; 112:1809–1820. [PubMed: 14638851]
35. Sasaki K, Tsuno NH, Sunami E, Tsurita G, Kawai K, Okaji Y, Nishikawa T, Shuno Y, Hongo K, Hiyoshi M, Kaneko M, Kitayama J, Takahashi K, Nagawa H. Chloroquine potentiates the anti-cancer effect of 5-fluorouracil on colon cancer cells. BMC Cancer. 2010; 10:370. [PubMed: 20630104]
36. Seglen PO, Brinchmann MF. Purification of autophagosomes from rat hepatocytes. Autophagy. 2010; 6
37. Shi YH, Ding ZB, Zhou J, Hui B, Shi GM, Ke AW, Wang XY, Dai Z, Peng YF, Gu CY, Qiu SJ, Fan J. Targeting autophagy enhances sorafenib lethality for hepatocellular carcinoma via ER stress-related apoptosis. Autophagy. 2011; 7:1159–1172. [PubMed: 21691147]
38. Solomon VR, Lee H. Chloroquine and its analogs: a new promise of an old drug for effective and safe cancer therapies. Eur J Pharmacol. 2009; 625:220–233. [PubMed: 19836374]
39. Stern ST, Zolnik BS, McLeland CB, Clogston J, Zheng J, McNeil SE. Induction of autophagy in porcine kidney cells by quantum dots: a common cellular response to nanomaterials? Toxicol Sci. 2008; 106:140–152. [PubMed: 18632727]
40. Stover T, Kester M. Liposomal delivery enhances short-chain ceramide-induced apoptosis of breast cancer cells. J Pharmacol Exp Ther. 2003; 307:468–475. [PubMed: 12975495]
41. Stover TC, Sharma A, Robertson GP, Kester M. Systemic delivery of liposomal short-chain ceramide limits solid tumor growth in murine models of breast adenocarcinoma. Clin Cancer Res. 2005; 11:3465–3474. [PubMed: 15867249]
42. Tagaram HR, Divittore NA, Barth BM, Kaiser JM, Avella D, Kimchi ET, Jiang Y, Isom HC, Kester M, Staveley-O'Carroll KF. Nanoliposomal ceramide prevents in vivo growth of hepatocellular carcinoma. Gut. 2011; 60:695–701. [PubMed: 21193455]

43. van Vlerken LE, Duan Z, Little SR, Seiden MV, Amiji MM. Augmentation of therapeutic efficacy in drug-resistant tumor models using ceramide coadministration in temporal-controlled polymer-blend nanoparticle delivery systems. AAPS J. 2010; 12:171–180. [PubMed: 20143195]
44. Wei Y, Sinha S, Levine B. Dual role of JNK1-mediated phosphorylation of Bcl-2 in autophagy and apoptosis regulation. Autophagy. 2008; 4:949–951. [PubMed: 18769111]
45. White EJ, Martin V, Liu JL, Klein SR, Piya S, Gomez-Manzano C, Fueyo J, Jiang H. Autophagy regulation in cancer development and therapy. Am J Cancer Res. 2011; 1:362–372. [PubMed: 21969237]
46. Xie R, Nguyen S, McKeehan WL, Liu L. Acetylated microtubules are required for fusion of autophagosomes with lysosomes. BMC Cell Biol. 2010; 11:89. [PubMed: 21092184]
47. Yue Z, Jin S, Yang C, Levine AJ, Heintz N. Beclin 1 an autophagy gene essential for early embryonic development is a haploinsufficient tumor suppressor. Proc Natl Acad Sci U S A. 2003; 100:15077–15082. [PubMed: 14657337]
48. Zhou F, Yang Y, Xing D. Bcl-2 and Bcl-xL play important roles in the crosstalk between autophagy and apoptosis. FEBS J. 2011; 278:403–413. [PubMed: 21182587]
49. Zhou Q, Lui VW, Lau CP, Cheng SH, Ng MH, Cai Y, Chan SL, Yeo W. Sustained antitumor activity by co-targeting mTOR and the microtubule with temsirolimu s /vinblastine combination in hepatocellular carcinoma. Biochem Pharmacol. 2012; 83:1146–1158. [PubMed: 22285225]
50. Zolnik BS, Stern ST, Kaiser JM, Heakal Y, Clogston JD, Kester M, McNeil SE. Rapid distribution of liposomal short-chain ceramide in vitro and in vivo. Drug metabolism and disposition: the biological fate of chemicals. 2008; 36:1709–1715. [PubMed: 18490436]

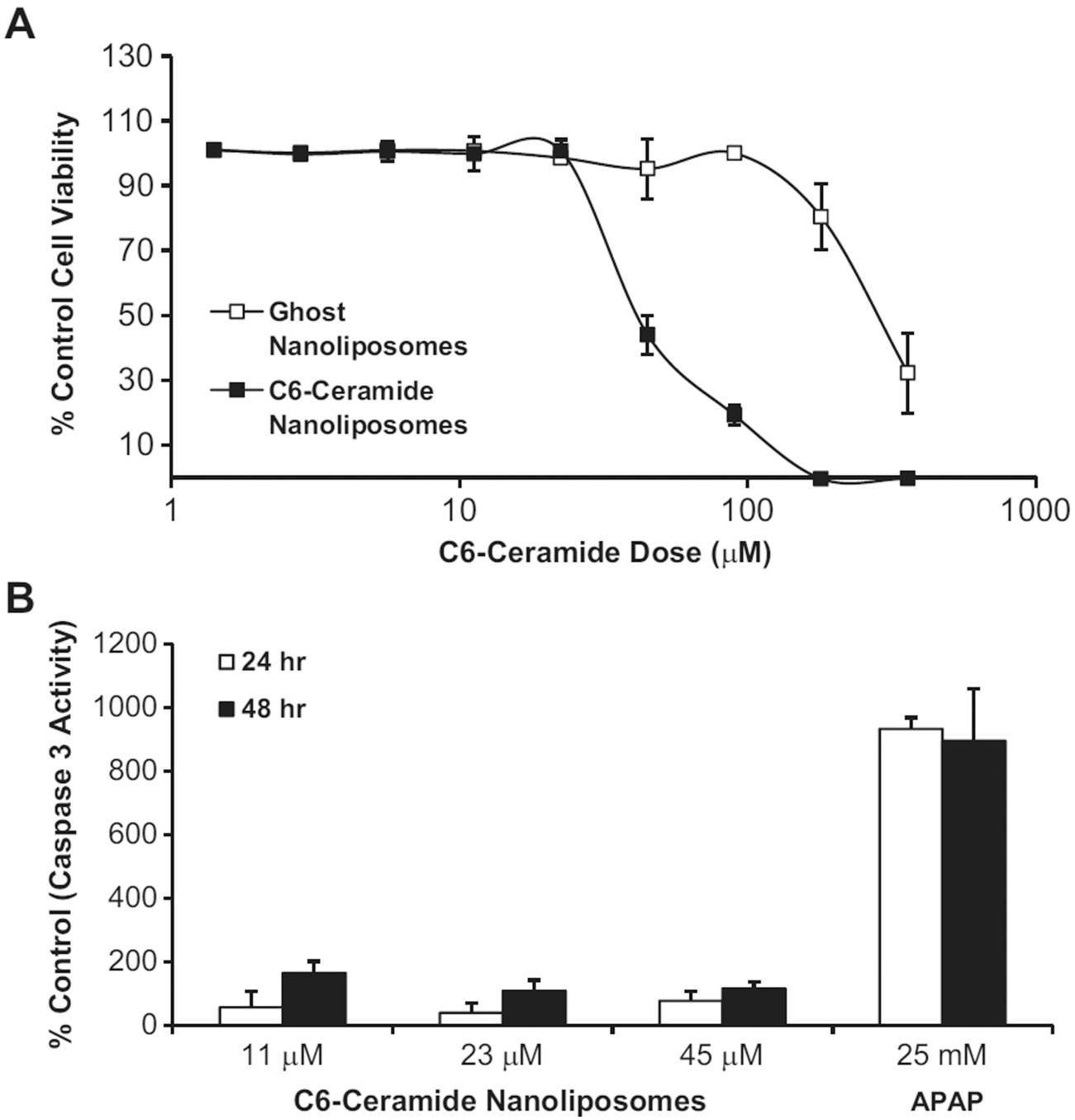

Figure 1.

Analysis of cytotoxic potency and apoptotic activity of C6-ceramide nanoliposomes in HepG2 cells. **A**. Cytotoxicity in HepG2 cells determined by the MTT assay. Data is presented as the % control cell viability, mean ± SD, *N*=3. HepG2 cells were treated for 48 h with varying concentrations of C6-ceramide nanoliposomes or an equivalent volume of ghost nanoliposomes. **B**. Caspase 3/7 activity in HepG2 cells. Cells were treated for 24 and 48 h with 11, 23, and 45 μM concentrations of C6-ceramide nanoliposomes. Acetaminophen (25 mM; APAP) was used as the positive control and cell culture media as a negative control. Data are presented as % negative control caspase 3/7 activity, mean ± SD of three individual samples.

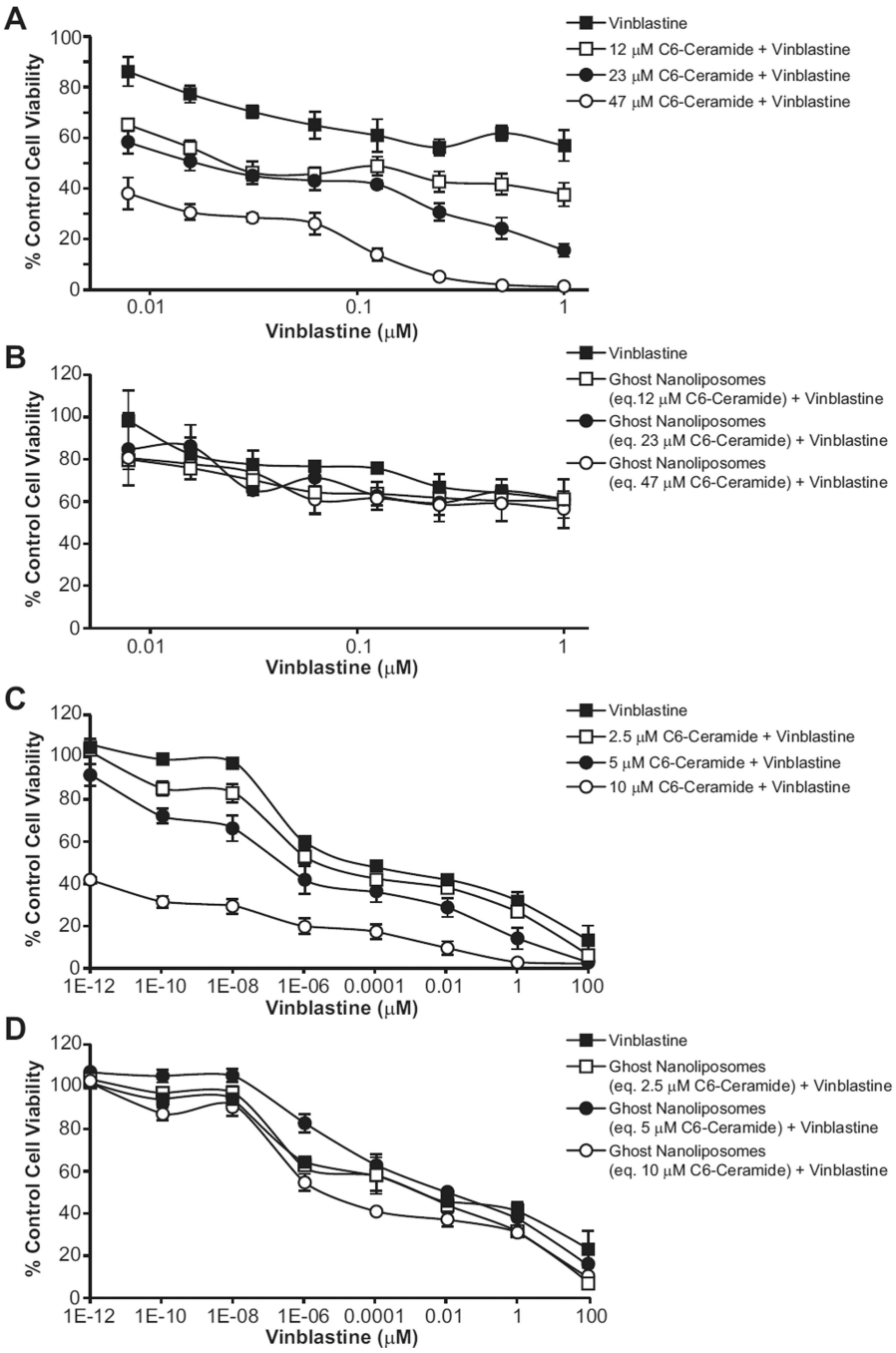

Figure 2.

Cytotoxicity assay of ghost or C6-ceramide nanoliposomes in combination with vinblastine in HepG2 and LS174T cells. HepG2 and LS174T cells were treated for 48 h with vinblastine (0.008–1 μ*M* for HepG2 cells and 10^{-12} – 10^{2} μM for LS174T cells) in cell culture media, alone or in combination with C6-ceramide nanoliposomes (12, 24, and 47 μM for HepG2 cells and 2.5, 5.0, and 10 μM for LS174T cells), or equivalent dilution of ghost nanoliposomes. Displayed are data for C6-ceramide nanoliposomes **(A and C)** and ghost nanoliposomes **(B and D)**. in HepG2 and LS174T cells, respectively. Cytotoxicity was determined by the MTT assay for HepG2 cells and SRB assay for LS174T cells, as

described in the Materials and Methods. Data represents the % media control, mean ± SD, *N*=3.

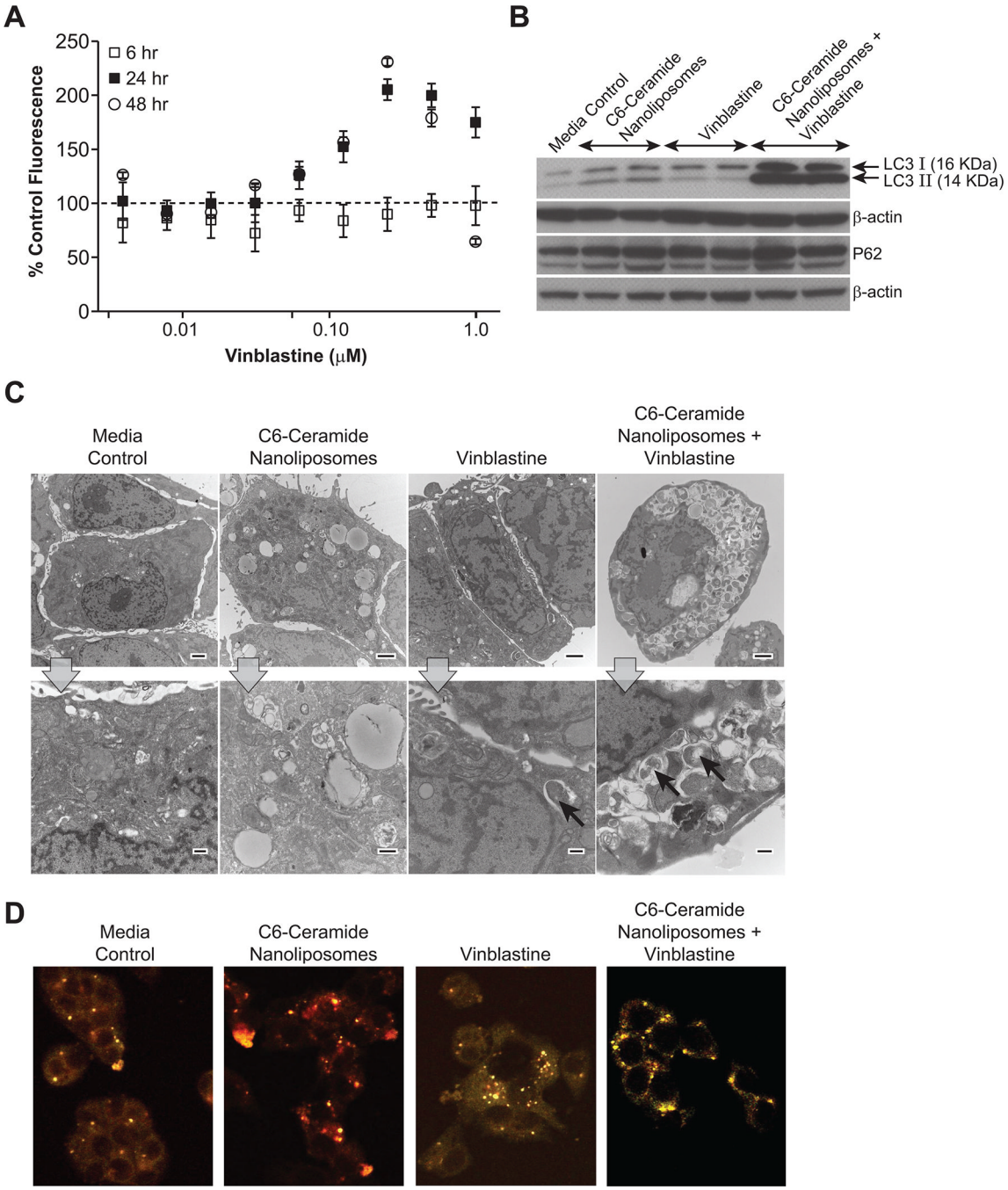

Figure 3.

Autophagy induction by combination treatment. **A**. Evaluating autophagic response by the Lysotracker Red dye uptake assay. HepG2 cells were treated for 6, 24, or 48 h with 24 μM C6-ceramide nanoliposomes in combination with vinblastine(0.008 – 1 μM). Data is plotted as the percent control Lysotracker Red fluorescence normalized to Celltracker Green fluorescence. Values presented are the mean ± SD of three individual samples. **B**. LC3, P62 and β-actin immunoblot analysis in HepG2 cells. HepG2 cells were treated for 24 h with cell culture media alone (negative control), 47 μM of C6-ceramide nanoliposomes, 0.2 μM of vinblastine, or C6-ceramide nanoliposomes in combination with vinblastine. The

experiments were performed in duplicate. **C**. TEM photomicrographs of HepG2 cells. HepG2 cells were treated with cell culture media (negative control), 47 μM C6-ceramide nanoliposomes, 0.2 μM vinblastine, or 47 μM C6-ceramide nanoliposomes in combination with 0.2 μM vinblastine. A representative low (top row) and high (bottom row) magnification photomicrograph for each treatment is displayed. Arrows indicate autophagic vacuoles. Top row images, scale bar = *2μm* and magnification = 1500x; bottom row images, scale bar = 500 nm and magnification = 6000x. **D**. Representative images of stably transfected mCherry-GFP-LC3 HepG2 cells. Cells were treated for 6 h with media (negative control), 12 μM C6-ceramide nanoliposomes alone, 0.1 μM vinblastine alone, and 12 μM C6-ceramide nanoliposomes in combination with 0.1 μM vinblastine.

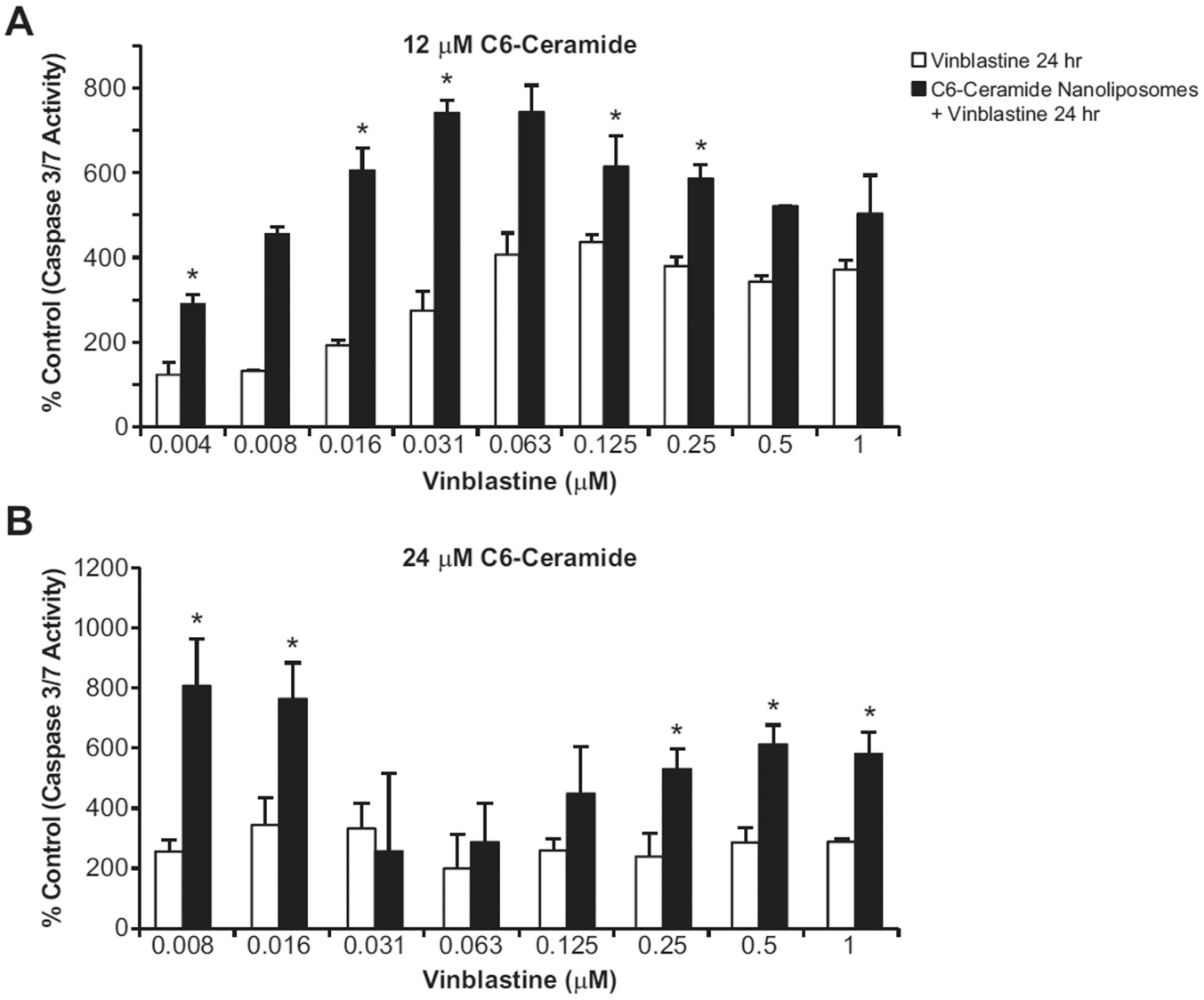

Figure 4.

Analysis of caspase 3/7 activity in HepG2 cells. HepG2 cells were treated for 24 h with cell culture media (negative control) or vinblastine (0.008 – 1 μM) alone, or in combination with 12 (**A**) or 24 μM (**B**) C6-ceramide nanoliposomes. Data are presented as % negative control caspase 3/7 activity. Data presented is the mean ± SD of three individual samples. * indicates statistically significance in comparison to vinblastine treatment alone $p<0.05$ (ANOVA with Dunnett's T test).

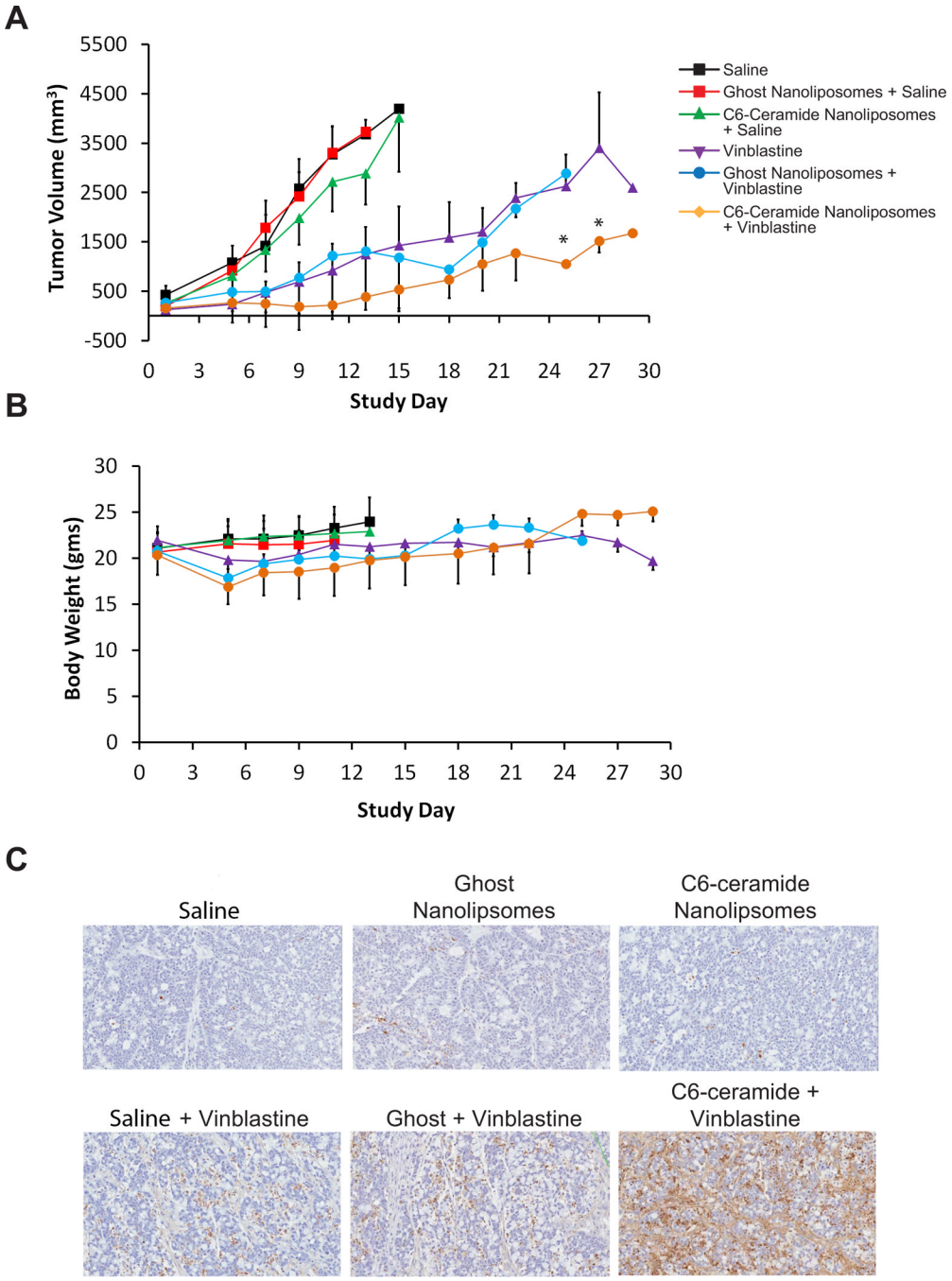

Figure 5.

Antitumor activity of C6-ceramide nanoliposomes in combination with vinblastine in an LS174T xenograft model. **A**. Tumor growth in response to C6-ceramide nanoliposome and vinblastine combination therapy or single agent therapy, in a subcutaneously implanted LS174T human colon cancer model. Asterisks indicate significantly different from vinblastine treatment group (20 mg/kg), $p<0.05$ (ANOVA, with post hoc comparisons by Duncan's multiple range test). **B**. Body weight over the study period by treatment group are presented, as an indicator of toxicity. Data represents mean ± SD. **C**. TUNEL staining of tumors from animals treated with saline (vehicle control), C6-ceramide or ghost

nanoliposomes alone, vinblastine alone, and C6-ceramide or ghost nanoliposomes in combination with vinblastine. Enhanced TUNEL staining of tumor sections by C6-ceramide in combination with vinblastine suggest increased apoptotic activity in comparison to the individual treatments and controls.

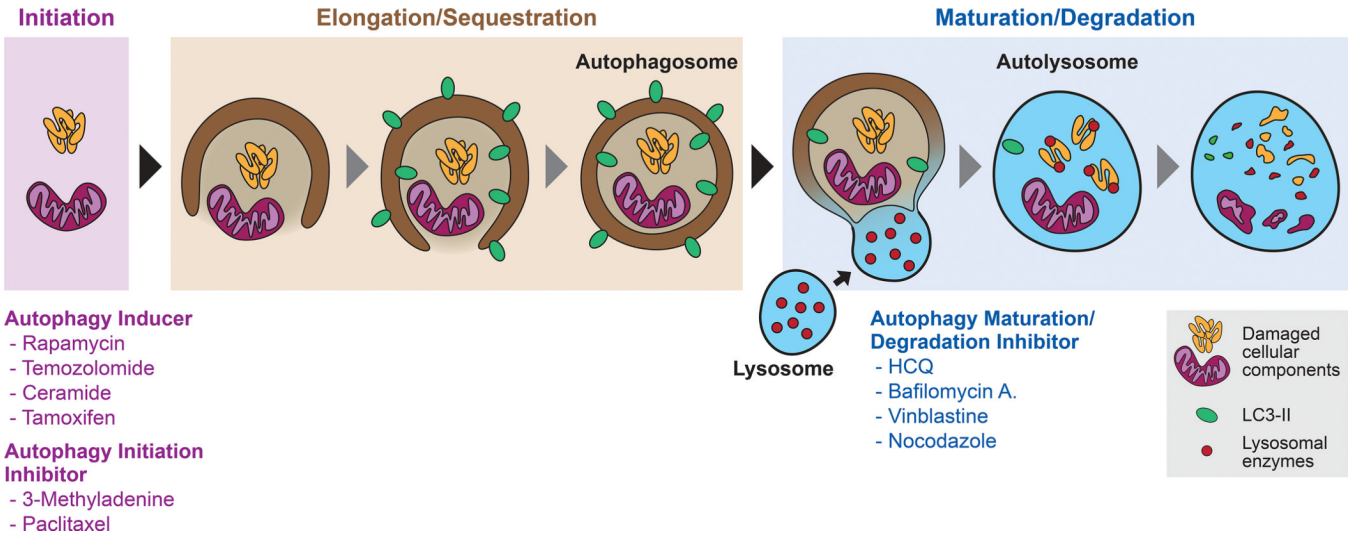

Figure 6.

Schematic representation of autophagy and therapeutic intervention strategies. Treatment of cancer cells with autophagy inducers (e.g., rapamycin, ceramide, tamoxifen) or autophagy initiation inhibitors (e.g., 3-methyladenine, paclitaxel) regulate the initiation step of autophagy. Autophagy involves the initial formation of double membrane autophagosomes and sequestering of cellular components (e.g., aggregated cellular proteins and damaged organelles). Maturation of autophagosome requires the fusion with lysosomes to form autolysosomes, which is followed by degradation of cellular components by lysosomal enzymes. Autophagy maturation/degradation inhibitors (e.g., hydroxychloroquine, bafilomycin A_1, vinblastine, nocodazole) block autophagosome fusion with lysosomes, resulting in blockade of autophagy flux and the accumulation of autophagic vacuoles.